*Inorg. Chem.* **2007**, *46*, 1277−1282

# Novel Vanadium(IV) Oxyfluorides with 'Spin-Ladder'-Like Structures, and Their Relationship to $(VO)_2P_2O_7$

**David W. Aldous,[†] Richard J. Goff,[†] J. Paul Attfield,[‡] and Philip Lightfoot*[,†]**

*EaStChem, School of Chemistry, University of St. Andrews, St. Andrews, Fife KY16 9ST, U.K., and EaStChem, School of Chemistry and Centre for Science at Extreme Conditions, University of Edinburgh, Edinburgh, EH9 3JJ, U.K.*

Received September 13, 2006

Three novel vanadium(IV) oxyfluorides have been prepared by hydrothermal synthesis. All three materials feature 'ladder'-like chains of edge- and corner-sharing V(O/F) octahedra, topologically similar to those in $(VO)_2P_2O_7$. $CsVOF_3$ and $RbVOF_3$ are isostructural, whereas in $(bpeH_2)_{1/2}[VOF_3]$ (bpe = *trans*-1,2-bis(4-pyridyl)-ethylene) inclusion of the organic structure-directing agent affects both the conformation of the ladders and their packing within the unit cell. Magnetic susceptibility data for each of the new materials have been fitted using a spin-1/2 Heisenberg antiferromagnetic chain model, which shows that the predominant magnetic interactions act along the 'legs' of the ladder, with negligible interactions both along the 'rungs' and between neighboring chains. This behavior contrasts markedly with that of $(VO)_2P_2O_7$ itself.

## Introduction

The search for novel transition metal oxyfluorides is of interest since the differing bonding natures of the M−O bond and the M−F bond give rise to dramatic variations in and, potentially, fine control of the physical properties of the resulting materials. In very general terms the more covalent M−O bond typically results in enhanced electronic transport and magnetic interactions, whereas the more ionic M−F bond results in enhanced optical properties due to the wider band gaps and increased transparency range. An early review by Chamberland summarized some of these features, together with the general structural chemistry of transition metal oxyfluorides.[1] In addition to the differing electronic features of the M−X bonding above, Poeppelmeier and colleagues have exploited the bonding within the metal oxyfluoride polyhedral unit in a more purely structural sense, in order to 'crystal-engineer' novel coordination polymers, with desirable structural features.[2,3] Vanadium oxides have a particularly rich structural chemistry, driven on one hand by their potential applications in, for example, lithium battery technology and oxidative catalysis, and on the other hand by the diverse chemical and structural proclivities of vanadium itself, whereby vanadium−oxygen environments vary from 4- to 5- to 6-coordinate while the vanadium oxidation state varies from +5 to +3. A beautiful summary and classification of the structural chemistry of vanadium oxides has been given by Zavalij and Whittingham.[4] The structural chemistry of vanadium oxyfluorides (VOFs) is much less well-developed than that of the corresponding oxides. A noncomprehensive summary has been given in Nakajima et al.[5] A search of the Inorganic Crystal Structure Database (ICSD) reveals 26 VOFs containing either alkali metal or ammonium cations (Table 1); in addition, a few organically templated VOFs are also known, such as those incorporating lutidinium,[21] tetramethylammonium,[22] and ethylenediammonium.[23]

Our main motivation in this field is to expand the range of known VOFs, in particular by using organic cations as structure-directing agents, in order to develop novel structural building units which in the longer term we may seek to

* To whom correspondence should be addressed. E-mail: pl@st-and.ac.uk.
[†] University of St. Andrews.
[‡] University of Edinburgh.

(1) Chamberland, B. L. In *Inorganic Solid Fluorides*; Hagenmuller, P., Ed.; Academic Press: London, 1985.
(2) Norquist, A. J.; Heier, K. R.; Stern, C. L.; Poeppelmeier, K. R. *Inorg. Chem.* **1998**, *37*, 6495.
(3) Welk, M. E.; Norquist, A. J.; Stern, C. L.; Poeppelmeier, K. R. *Inorg. Chem.* **2000**, *39*, 3946.
(4) Zavalij, P. Y.; Whittingham, M. S. *Acta. Crystallogr.* **1999**, *B55*, 627.
(5) *Advanced Inorganic Fluorides: Synthesis, Characterization and Applications*; Nakajima, T., Zemva B., Tressaud A., Eds.; Elsevier Science: New York, 2000.
(6) Pausewang, G. *Z. Anorg. Allg. Chem.* **1971**, *381*, 189.
(7) Stomberg, R. *Acta. Chem. Scand. Ser. A, Phys. Inorg. Chem.* **1986**, *40*, 325.

10.1021/ic0617386 CCC: $37.00 
Published on Web 01/26/2007

**Table 1.** Previously Characterized Alkali Metal Vanadium Oxyfluorides

| chemical formula | structure type | oxidation state | ref |
|---|---|---|---|
| $Na_3VOF_5$[a] | monomer | IV | 6 |
| $Na_2VOF_5$ | monomer | V | 7 |
| $NaVO_2F_2$ | linear chain | V | 8 |
| $Na_6(H_6V_{12}O_{30}F_2)\cdot 22H_2O$ | polyanionic | IV | 9 |
| $NaV_2O_4F$ | layered | IV | 10 |
| $K_2VO_2F_3$ | zigzag chain | V | 11 |
| $KVOF_4$ | zigzag chain | V | 12 |
| $K_2VOF_4$ | zigzag chain | IV | 13 |
| $K_2VO_2F_3$ | zigzag chain | V | 7 |
| $RbVOF_4(H_2O)$ | monomer | IV | 4 |
| $Rb_2VOF_4$ | zigzag chain | IV | 15 |
| $Cs_2VOF_4(H_2O)$ | monomer | IV | 16 |
| $Cs_2VOF_4(H_2O)$ | monomer | IV | 17 |
| $Cs_3V_2O_2F_7$ | dimer | IV | 6 |
| $CsVOF_4$ | zigzag chain | V | 18 |
| $CsVOF_3\cdot 1/2H_2O$ | complex chain | IV | 19 |
| $Cs_3V_2O_4F_5$ | linear chain | V | 20 |

[a] And analogues with composition $A_2A'VOF_5$ (A = K, Rb, Cs; A′ = Li, Na, K, Rb).

control and direct toward the rational synthesis of functional VOFs, for example, for magnetic or optical applications. We have prepared a variety of organically templated VOFs, the first of which[23] exhibits a polar crystal structure and corresponding second-harmonic generation (SHG) properties. In parallel with our exploratory work in organically templated systems, we have also prepared several novel VOFs incorporating alkali metals. Two of these, $RbVOF_3$ and $CsVOF_3$, exhibit a novel ladder-like polymeric $[VOF_3]^-$ chain which is topologically closely related to the chain seen in the 'spin-ladder' phase $(VO)_2P_2O_7$[24,25]. Remarkably, the same type of chain has also been isolated in an otherwise unrelated, organically templated material $(bpeH_2)_{1/2}[VOF_3]$ (bpe = *trans*-1,2-bis(4-pyridyl)-ethylene). The syntheses, crystal structures, and magnetic characterization of these three new VOFs are presented herein.

## Experimental Section

$CsVOF_3$, $RbVOF_3$, and $(bpeH_2)_{1/2}[VOF_3]$ were all synthesized hydrothermally. $(bpeH_2)_{1/2}[VOF_3]$ was made in a 27 mL Teflon-lined stainless steel autoclave at 160 °C, while $CsVOF_3$ and $RbVOF_3$ were made in a 30 mL polypropylene bottle at 100 °C. A general scheme for synthesis is shown below.

$V_2O_5$ (0.182 g, $1.00 \times 10^{-3}$ mol) was weighed into a 30 mL polypropylene bottle and dissolved with 1 mL ($6.2 \times 10^{-2}$ mol) of 48% HF at room temperature for 5 min. To the resultant solution 5 mL ($2.78 \times 10^{-3}$ mol) of water was added (1 mL ($5.56 \times 10^{-4}$ mol) in the case of $CsVOF_3$ and $RbVOF_3$) along with 5 mL ($8.0 \times 10^{-2}$ mol) of ethylene glycol, creating an orange solution. This solution was transferred to the autoclave (or kept in the polypropylene bottle in the case of $CsVOF_3$ and $RbVOF_3$) to which $3 \times 10^{-3}$ mol of templating species (CsCl, RbCl, or dpe) was added. The reaction was then heated to the required temperature for 24 h and allowed to cool to room temperature. The products were filtered, washed with water, and dried at 60 °C in air to give blue, dark blue, and green needle-like crystals for $CsVOF_3$, $RbVOF_3$, and $(bpeH_2)_{1/2}[VOF_3]$, respectively.

Further experiments involving a variety of different temperatures and reactant ratios were explored; results of these reactions will be reported in future publications.

**Crystallography.** Single-crystal X-ray diffraction data were collected with either a Bruker SMART system (for $CsVOF_3$ and $RbVOF_3$) or a Rigaku Mercury CCD (for $(bpeH_2)_{1/2}[VOF_3]$) with silicon-monochromated synchrotron radiation (station 9.8 at CCLRC Daresbury Laboratory) or graphite-monochromated Mo $K_\alpha$ radiation, respectively. All datasets were corrected for absorption via multiscan methods. The structures were solved by direct methods and refined by full-matrix least-squares techniques using the SHELXS/SHELXL packages. All structures were checked for missing symmetry elements with PLATON, and the final refinement includes anisotropic displacement for all non-hydrogen atoms, except the bpe moiety, which was refined isotropically, with 50:50 disorder around the 2-fold axis. Hydrogen atoms were fixed and refined using a riding model with isotropic displacement parameters. Further crystallographic details are given in Table 2.

**Magnetic Measurements.** Magnetic data were measured on a Quantum Design MPMS SQUID. Data were recorded in 5000 Oe field while warming the sample from 2 to 334 K in 4 K steps, following consecutive zero field cooling (ZFC) and field cooling (FC) cycles.

## Results and Discussion

**Crystal Structures.** Despite the existence of a wide range of alkali metal vanadium oxyfluorides (Table 1), there are no previously known compounds of the $AVOF_3$ composition. More interestingly, the occurrence of extended-connectivity −V−(O/F)−V− lattices among such compounds is relatively rare.

$CsVOF_3$ and $RbVOF_3$ are isomorphous and consist of ladder-like chains of edge- and corner-sharing $[VOF_1F_{4/2}]$ octahedra, such that within each octahedral unit four F atoms bridge adjacent V centers and one F and one O atom are terminal. The asymmetric unit consists of only one V atom, three F atoms, one O, and one Cs or Rb. A detail of the ladder arrangement is shown in Figure 1. The local octahedral environment around the V atom is highly distorted, as is typical for V(IV) in oxyfluorides; in particular the terminal 'vanadyl' V=O group and *trans*-F have, respectively, short and long lengths. The bond lengths are presented in Table 3, together with the corresponding bond valence sums, which support the assignment of $V^{4+}$ (confirmed by the magnetic data).


(8) Crosnier-Lopez, M. P.; Duroy, H.; Fourquet, J. L.; Abrabri, M. *Eur. J. Solid State Inorg. Chem.* **1994**, *31*, 957.
(9) Mueller, A.; Rohlfing, R.; Krickemeyer, E.; Boege. *Angew. Chem.* **1993**, *105*, 909.
(10) Varpy, A.; Galy, J. *Bull. Soc. Fr. Min. Crist.* **1971**, *94*, 24.
(11) Ryan, R. R.; Mastin, S. H.; Reisfeld, M. J. *Acta. Crystallogr.* **1971**, *B27*, 1270.
(12) Rieskamp, H.; Mattes, R. *Z. Anorg. Allg. Chem.* **1973**, *401*, 158.
(13) Waltersson, K.; Karlson, B. *Cryst. Struc. Comm.* **1978**, *7*, 459.
(14) Schabert, M.; Pausewang, G.; Massa, W. *Z. Anorg. Allg. Chem.* **1983**, *506*, 169.
(15) Schabert, M.; Pausewang, G. *Z. Naturforsch.* **1985**, *40*, 1437.
(16) Waltersson, K. *J. Solid State Chem.* **1979**, *29*, 195.
(17) Mattes, R.; Foerster, H. *J. Solid State Chem.* **1982**, *45*, 154.
(18) Bushnell, G. W.; Moss, K. C. *Can. J. Chem.* **1972**, *50*, 3700.
(19) Waltersson, K. *J. Solid State Chem.* **1979**, *28*, 121.
(20) Mattes, R; Forster, H. *J. Less Comm. Metals* **1982**, *87*, 237.
(21) Demsar, A.; Leban, I.; Giester, G. *Acta. Chim. Slov.* **2002**, *49*, 259.
(22) Darriet, J.; Xu, Q.; Tressaud, A. *Acta. Crystallogr.* **1987**, *C43*, 224.
(23) Stephens, N. F.; Buck, M.; Lightfoot, P. *J. Mater. Chem.* **2005**, *15*, 4298.
(24) Johnston, D. C.; Johnson, J. W.; Goshorn, D. P.; Jacobson, A. J. *Phys. Rev. B.* **1987**, *35*, 219.
(25) Koo, H. J.; Whangbo, M. H.; VerNooy, P. D.; Torardi, C. C.; Marshall, W. J. *Inorg. Chem.* **2002**, *41*, 4664.

**Table 2.** Crystallographic Data for the Present Series

| | | | |
|---|---|---|---|
| molecular formula | $CsVOF_3$ | $RbVOF_3$ | $[C_{12}H_{12}N_2]_{0.5}[VOF_3]$ |
| cryst syst | orthorhombic | orthorhombic | monoclinic |
| space group | *Pbam* (No. 55) | *Pbam* (No. 55) | *C*2/*c* (No. 15) |
| *a* (Å) | 9.004(2) | 8.559(4) | 11.972(2) |
| *b* (Å) | 11.703(2) | 11.526(6) | 15.663(3) |
| *c* (Å) | 3.909(7) | 3.859(2) | 7.581(2) |
| $\beta$ (deg) | | | 95.010(3) |
| *V* (Å$^3$) | 411.9(1) | 380.7(3) | 1416.1(5) |
| *Z* | 4 | 4 | 8 |
| total/unique reflns | 2846/414 | 2152/580 | 5136/1506 |
| independent reflns $>2\sigma(I)$ | 323 | 340 | 989 |
| fw | 256.85 | 209.41 | 216.05 |
| *T* (°C) | −123(2) | −180 | −123(2) |
| $\lambda$ (Å) | 0.8462 | 0.7107 | 0.8462 |
| $\rho_{calcd}$ (g/cm$^3$) | 4.142 | 3.654 | 2.017 |
| R1 [$I > 2\sigma(I)$] | 0.038 | 0.061 | 0.071 |
| wR2 [$I > 2\sigma(I)$] | 0.091 | 0.141 | 0.163 |

$(bpeH_2)_{1/2}[VOF_3]$ was prepared during a more general survey of the hydrothermal chemistry of vanadium oxyfluorides incorporating organic structure-directing agents, to be discussed in future papers. To our surprise, its crystal structure exhibits the same type of ladder chain as $CsVOF_3$ and $RbVOF_3$. In this case, the symmetry of the chain is lowered in order to accommodate the bulkier countercation, such that the chain-repeat distance (ie. *c* axis) is effectively 'doubled', due to its 'zigzag' nature (Figures 1 and 2).

The ladder-like chain present in all three of our compounds bears a striking resemblance to that in vanadyl pyrophosphate, $(VO)_2P_2O_7$,[24,25] also shown in Figure 1. $(VO)_2P_2O_7$ has been studied intensively in recent years due to both its catalytic activity and its interesting magnetic properties. The latter depend critically on the detailed nature of the *intra*ladder V−O bonding and also on the secondary *inter*ladder interactions. Therefore, a closer comparison of these particular features of the present compounds, together with those in $(VO)_2P_2O_7$, is merited. Within the ladder, the most obvious difference is that the bonding between neighboring V centers is mediated by oxygen in $(VO)_2P_2O_7$ but by fluorine in the presents cases. In addition, the very short 'vanadyl' V═O bond is terminal in our $[VOF_3]^-$ chains but bridging in $(VO)_2P_2O_7$. V−V interactions within the $[VOF_3]^-$ ladders are in the range 3.31−3.34 Å for the edge-shared octahedra ('rungs' of the ladder) and 3.79−3.91 Å for the corner-shared polyhedra ('legs' along the ladder) (Table 3). In $(VO)_2P_2O_7$, the distortion around each vanadyl group is so extreme (V═O bonds as short as 1.58 Å, with trans V−O bonds as long as 2.35 Å) that the key V−V interactions are generally regarded as a dimeric unit of edge-shared square pyramids forming the rungs, although the resulting V−V distances are nevertheless in the same range as those observed in the present series: around 3.2−3.3 Å for the rungs and 3.8−3.9 Å for the legs.

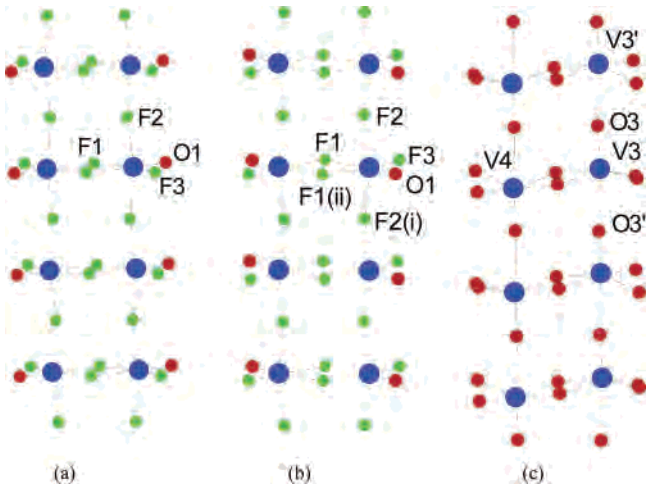


**Figure 1.** $[VOF_3]$ ladder in (a) $CsVOF_3$ and (b) $(bpeH_2)_{1/2}[VOF_3]$ and (c) the corresponding ladder in $(VO)_2P_2O_7$. Note the differing orientations of the 'vanadyl' O atoms O1 (a and b) and O3 (c).

Interladder interactions differ considerably among the three different structure types, as shown by the projections of the unit cells in Figure 3. Adjacent ladders in $(VO)_2P_2O_7$ are connected by strong covalent bonds through pyrophosphate groups, leading to medium-range V−V interladder interactions (around 5.15 Å). The corresponding interactions in our structures are mediated via $Cs^+$ or $Rb^+$ cations, or by H-bonded $[dpeH_2]^{2+}$ moieties, leading to longer V−V interladder contacts (e.g., 5.29 and 5.85 Å for $RbVOF_3$, 8.44 and 8.87 Å for $(bpeH_2)_{1/2}[VOF_3]$). The local interladder contacts in $CsVOF_3$, mediated by $Cs^+$, are shown in Figure 4. In the case of $(bpeH_2)_{1/2}[VOF_3]$, the interchain interactions are mediated by H-bonding from the N−H group to the fluorine atoms within the chain; an expanded view of this is shown in Figure 5, and geometry details are shown in Table 3.

**Magnetic Susceptibilities.** At high temperatures, the magnetic susceptibilities follow a Curie−Weiss law. From fits of the $\chi$ vs *T* above 150 K, values of $\mu_{eff}$ ($\mu_B$) and $\theta$ (K) were derived (Table 4). These values confirm that $S = 1/2$ $V^{4+}$ is present in all the compounds, with predominantly antiferromagnetic interactions between spins. The deviation from the spin-only value of 1.73 $\mu_B$ in the bpe derivative may be due to a small orbital contribution, arising from the smaller degree of off-center displacement of the vanadium in this case. In the case of $RbVOF_3$, the lower-than-spin-only value suggests that short-range antiferromagnetic pairing interactions are significant up to ~300 K, and a higher temperature range would be needed to obtain an accurate $\mu_{eff}$.

All three materials exhibit characteristics of short-range antiferromagnetic order in the $\chi$ vs *T* data, with broad maxima at ~70 K for $CsVOF_3$ and $RbVOF_3$ and around 25 K

**Table 3.** Selected Bond Distances (Å) and Angles (deg) and Bond Valence Sums (Σ, v.u.)

| $CsVOF_3$ | | $RbVOF_3$ | | $(bpeH_2)_{1/2}[VOF_3]$ | |
|---|---|---|---|---|---|
| V1−O1 | 1.600(8) | V1−O1 | 1.584(12) | V1−O1 | 1.690(4) |
| V1−F1 | 1.965(6) | V1−F1 | 1.958(10) | V1−F1 | 2.022(3) |
| V1−F1 | 2.168(6) | V1−F1 | 2.160(9) | V1−F1 | 2.108(3) |
| V1−F2 (×2) | 1.9718(9) | V1−F2 (×2) | 1.948(2) | V1−F2 | 1.966(3) |
| V1−F3 | 1.898(6) | V1−F3 | 1.893(9) | V1−F2 | 1.968(3) |
| | | | | V1−F3 | 1.789(4) |
| V1−F1−V1 | 106.2(3) | V1−F1−V1 | 107.1(4) | V1−F1−V1 | 107.9(1) |
| V1−F2−V1 | 164.8(4) | V1−F2−V1 | 164.1(9) | V1−F2−V1 | 149.3(2) |
| Cs1−F1 (×2) | 3.023(4) | Rb1−F1 (×2) | 2.823(7) | | |
| Cs1−F3 (×2) | 3.076(4) | Rb1−F3 (×2) | 2.866(7) | | |
| Cs1−F3 (×2) | 3.157(4) | Rb1−F3 (×2) | 3.208(8) | | |
| Cs1−O1 (×2) | 3.183(6) | Rb1−O1 (×2) | 2.953(9) | | |
| Cs1−F2 | 3.277(6) | Rb1−F2 | 3.18(2) | | |
| Cs1−F2 | 3.594(6) | | | | |
| Cs1−O1 | 3.690(6) | | | | |
| Σ (V1) | 3.96 | 4.12 | | 3.81 | |
| Σ (M1) | 1.22 | 1.06 | | − | |
| Σ (O1) | 1.80 | 2.04 | | 1.30 | |
| Σ (F1) | 0.93 | 1.17 | | 0.75 | |
| Σ (F2) | 1.07 | 1.09 | | 0.97 | |
| Σ (F3) | 0.83 | 0.99 | | 0.78 | |
| V−V (rung) | 3.31 | | 3.32 | 3.34 | |
| V−V (leg) | 3.91 | | 3.86 | 3.79 | |
| V−V (interladder) | 5.82, 5.99 | | 5.29, 5.85 | 8.44, 8.87 | |

hydrogen bonding in $(bpeH_2)_{1/2}[VOF_3]$

| D−H | *d*(D−H) | *d*(H···A) | ∠DHA | *d*(D···A) | *A* |
|---|---|---|---|---|---|
| N1−H1 | 0.86 | 2.10 | 132.8 | 2.756 | F1 [ *x*, −y + 1, *z* − 1/2] |
| N1−H1 | 0.86 | 2.14 | 128.1 | 2.756 | F1 [ −*x* + 1, −*y* + 1, −*z* + 1] |
| N2−H2 | 0.86 | 2.16 | 145.0 | 2.903 | F2 [ −*x* + 1, −*y*, −*z* + 1] |
| N2−H2 | 0.86 | 2.27 | 130.1 | 2.903 | F2 [ *x*, −*y*, *z* − 1/2] |
| N2−H2 | 0.86 | 2.36 | 115.3 | 2.838 | F1 [ *x*, *y* − 1, *z*] |
| N2−H2 | 0.86 | 2.41 | 110.8 | 2.838 | F1 [ −*x* + 1, *y* − 1, −*z* + 1/2] |

for $(bpeH_2)_{1/2}[VOF_3]$. A sharp upturn in $\chi$ at low $T$ evidences a small amount of paramagnetic impurity (<1%) in all the samples. The crystal structures show that these three materials contain two-leg ladders of $S = 1/2$ vanadyl groups, in which distinct superexchange pathways along the chains (legs), $J_1$, and dimers (rungs), $J_2$, are present. If $J_2 \gg J_1$, then the magnetic behavior should approximate to that of a Bleaney−Bowers dimer,[26] whereas if $J_1 \gg J_2$, then the susceptibility will follow a one-dimensional model such as the Heisenberg $S = 1/2$ antiferromagnetic chain.[27] If the interactions are of comparable strength, then a fuller $S = 1/2$ spin ladder[28] treatment would be needed.

The Bleaney−Bowers and Heisenberg chain models were fitted to the molar susceptibilities after diamagnetic corrections. A Curie−Weiss term $\chi_{LT}$ was also included in each fit to allow for paramagnetic impurity contributions. The full expression for the Heisenberg chain model is then:[27]

$$\chi(T) = \chi_{1D}(T) + \chi_{LT}(T)$$

with

$$\chi_{1D}(T) = (N_A\mu^2{}_{eff}/3k_BT)[(1 + 0.08516x + 0.23351x^2)/(1 + 0.73382x + 0.13696x^2 + 0.53568x^3)]$$

where $x = |J|/k_BT$ and $\chi_{LT}(T) = C/(T - \theta)$.

Note that, due to the presence of significant paramagnetic impurities, it is not possible to derive reliable values of $\mu_{eff}$ or $g$ from the Heisenberg fits. The Heisenberg chain model generally gave a better fit than the Bleaney−Bowers model, as shown for $CsVOF_3$ in Figure 6. For $RbVOF_3$ (Figure 7), neither fit is entirely satisfactory, although the Heisenberg model gives a better fit in the high-temperature limit, and a more complex interaction network may be present. We note from Table 3 that the nearest interladder V−V distance is significantly shorter in $RbVOF_3$ than in $CsVOF_3$, which may strengthen other exchange pathways. No significant improve-

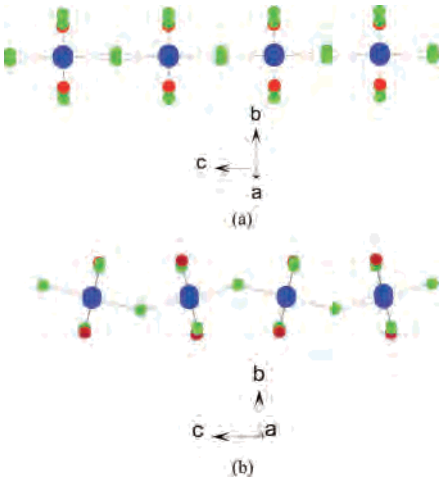


**Figure 2.** Projection along the 'rungs' of the $[VOF_3]$ ladder in (a) $CsVOF_3$ and (b) $(bpeH_2)_{1/2}[VOF_3]$, showing doubling of the *c* axis in (b) due to octahedral tilting.

(26) Carlin, R. L. *Magnetochemistry*; Springer: Berlin, 1986.
(27) Kaul, E. E.; Rosner, H.; Yushankai, V.; Sichelschmidt, J.; Shpanchenko, R. V.; Geibel, C. *Phys. Rev. B.* **2003**, *67*, 174417.
(28) Landee, C. P.; Turnbull, M. M.; Galeriu, C.; Giantsidis, J.; Woodward, F. M. *Phys. Rev. B.* **2001**, 63, 100402(R).

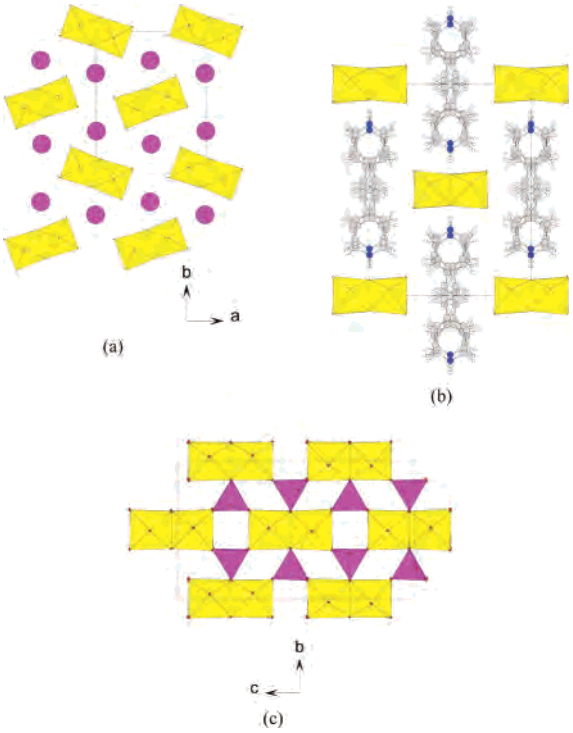


**Figure 3.** Unit cell projection along the $[VOF_3]$ ladder axis in (a) $CsVOF_3$, (b) $(bpeH_2)_{1/2}[VOF_3]$, and (c) $(VO)_2P_2O_7$.

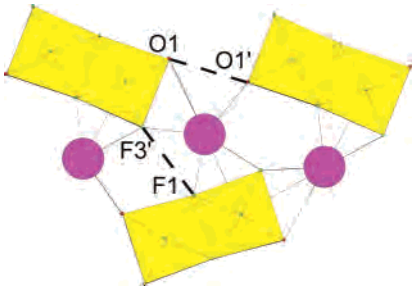


**Figure 4.** Local interchain communication in $CsVOF_3$. O1−O1′, 3.05 Å (corresponding V−V distance 5.82 Å); F1−F3′, 3.19 Å (corresponding V−V distance 5.99 Å).

ment was found by fitting more complex spin-ladder models to the $RbVOF_3$ data. Hence, we conclude that in general $J_1 \gg J_2$ in these materials. Values of $J_1$ derived from the Heisenberg chain model are given in Table 4. The corresponding $\chi$ vs $T$ fits are shown in Figures 6−8.

## Discussion and Conclusions

In broad terms, each of the present compounds displays a ladder-like structural feature reminiscent of the topology seen in $(VO)_2P_2O_7$. However, on closer inspection, there are fundamental differences between the two types of ladder and the interactions within and between them, which have significant effects on the magnetic properties of the materials. As discussed in the earlier section, the key differences are (i) that the V−V interactions are mediated by F rather than O, (ii) that the short vanadyl bond is terminal rather than *intra*chain, and (iii) that the interactions between neighboring ladders are mediated very differently. The second and third points are key, since (ii) determines which metal orbitals

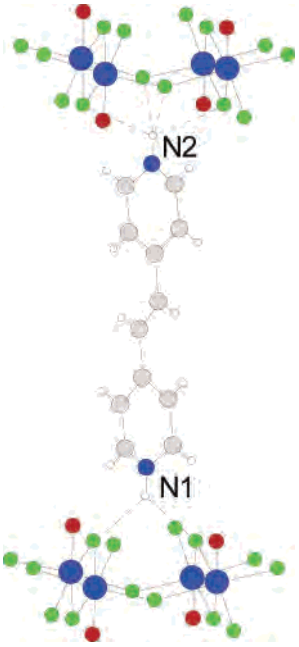


**Figure 5.** Local interchain communication in $(bpeH_2)_{1/2}[VOF_3]$. Note only one orientation of the disordered bpe moiety is shown.

**Table 4.** Magnetic Parameters

| | $CsVOF_3$ | $RbVOF_3$ | $(bpeH_2)_{1/2}[VOF_3]$ |
|---|---|---|---|
| $\mu_{eff}$ ($\mu_B$) | 1.79(4) | 1.39(4) | 1.91(5) |
| $\theta$ (K) | −122.9(3) | −92.2(5) | −27.4(7) |
| $J_1$ (K)[a] | −65.8(2) | −67(3) | −20.1(3) |

[a] Note that the Heisenberg expression provides $|J|$, and these values have been converted to '$-J$' by convention.

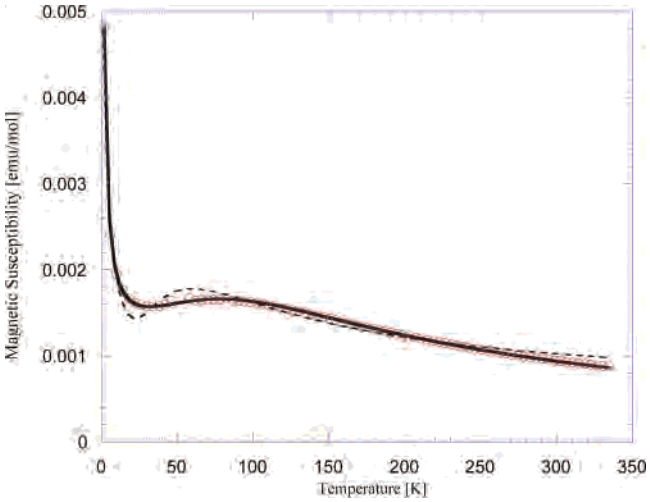


**Figure 6.** Bleaney−Bowers (dashed line) and Heisenberg (solid line) fits to $\chi(T)$ for $CsVOF_3$.

are involved in the magnetic exchange pathways within the ladder and (iii) dictates any potential for interladder effects.

The local $z$ axis is defined by the V═O bond, and the off-center displacement of the $V^{4+}$ within its octahedron splits the $t_{2g}$ orbitals, such that the $d_{xy}$ orbital lies lowest in energy and is singly occupied. In the case of $(VO)_2P_2O_7$, this then leads to favorable V−O $d\pi-p\pi$ superexchange within the dimers forming the ladder rungs, as well as significant O−O super-superexchange through the phosphate moieties, such that the overall antiferromgnetic chain occurs along the $c$

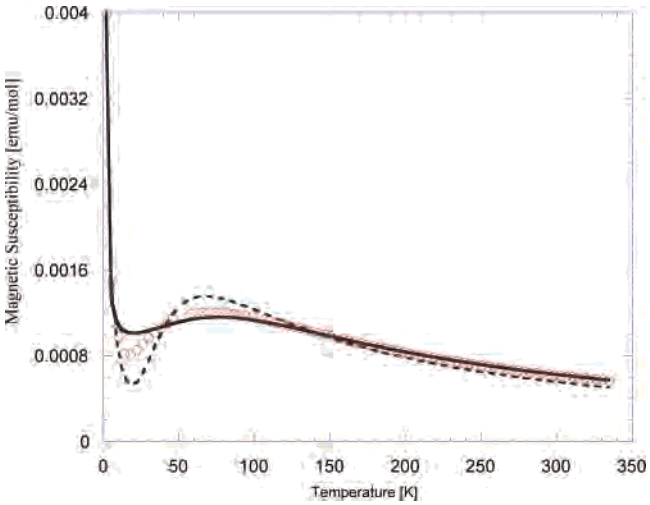


**Figure 7.** Bleaney−Bowers (dashed line) and Heisenberg (solid line) fits to $\chi(T)$ for $RbVOF_3$.

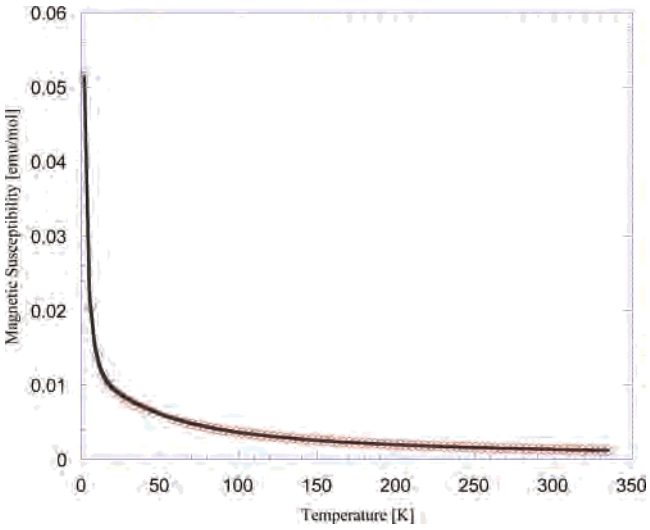


**Figure 8.** Heisenberg fit to $\chi(T)$ for $(bpeH_2)_{1/2}[VOF_3]$.

direction in $(VO)_2P_2O_7$ (Figure 3c), and *not* along the ladder direction, *a*. This surprising result is perhaps counterintuitive to a structural chemist and explains some of the earlier controversy[24,25,29] concerning the nature of $(VO)_2P_2O_7$, which has now been definitively characterized[30] as an alternating spin-1/2 Heisenberg chain, with two differing *J* values for *intra*dimer (rung) and *inter*dimer (i.e., *inter*ladder) interactions along *c*, i.e., there are no significant interactions along the legs of the 'ladder' at all!

In contrast, in the present compounds, V═O bonds, and hence the local *z* axes, lie exo to the ladder and therefore the $d_{xy}$ orbital has favorable $\pi$ overlap with the F atoms of the legs *along* the ladder direction but does not interact constructively by $\sigma$ overlap within the dimers forming the rungs. The *J* values derived from our Heisenberg fits therefore pertain to antiferromagnetic interactions *along* the ladder direction; the smaller *J* values for $(bpeH_2)_{1/2}[VOF_3]$ vs $CsVOF_3$ and $RbVOF_3$ can therefore be understood by the

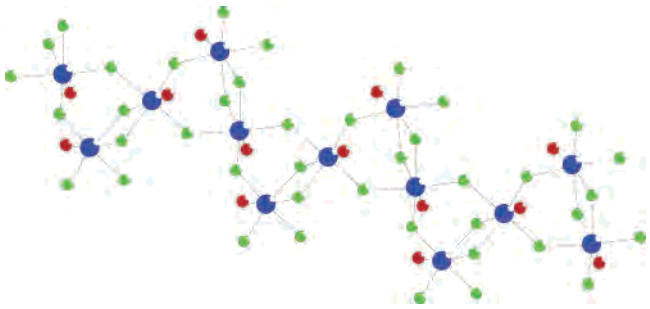

**Figure 9.** Complex V−O−F chain present in $CsVOF_3 \cdot 1/2H_2O$[19].

differing profiles of the ladders in projection (Figure 2); the zigzag nature of the V−F−V linkages inherently weakens this superexchange. In contrast to $(VO)_2P_2O_7$, therefore, the magnetic behavior of present materials *does* coincide more with the intuitive 'chemist's view' of the ladder-like structure, in that the obvious 'ladders' shown in Figure 1a and b do have magnetic interactions along their legs.

In Table 1 it can be seen that there is one further compound which displays a very similar composition to the present family, viz., $CsVOF_3 \cdot 1/2H_2O$[19]. The structure of this phase is quite different to that of the present $CsVOF_3$ and features a complex zigzag chain which includes two crystallographically distinct vanadium sites (Figure 9). Both sites have one terminal V═O group, but one has five bridging F sites, whereas the other has three bridging and two terminal F sites. This compound, together with several of the other Cs−V−O−F phases in Table 1, is prepared at room temperature, and the different products arise predominantly from different Cs/V ratios.[19] The main differences in synthesis between these earlier phases and the present, novel $CsVOF_3$ structure appear to be in the use of $Cs_2CO_3$ rather than CsCl as a Cs source and reduced vanadium oxides rather than just $V_2O_5$ as a vanadium source.

The present work presents some interesting pointers to future work in both chemistry and physics. On the one hand, the example of the Cs-based system above suggest that very subtle differences in reaction conditions can lead to a wide variety of compositions and structure types in such an apparently simple system. On the other hand, the fact that topologically similar 'ladder'-based structures can be prepared in systems as apparently unrelated as those based on Cs/Rb or bpe suggests that further exploratory work in vanadium oxyfluorides, using both inorganic and organic templates, would be very fruitful. The marked contrasts in magnetic behavior between the present materials and $(VO)_2P_2O_7$, despite at first sight being very similar in the structural chemistry sense, suggests that further, novel low-dimensional physics remains to be discovered in these chemically rich systems.

**Acknowledgment.** We thank Prof. Alex Slawin for assistance in collecting the diffraction data, Jason Farrell for help with the SQUID measurements, and the University of St. Andrews and EPSRC for funding.

**Supporting Information Available:** Crystallographic data in CIF format. This material is available free of charge via the Internet at http://pubs.acs.org.

IC0617386

(29) Barnes T.; and Riera, J. *Phys. Rev. B.* **1994**, *50*, 6817.
(30) Garrett, A. W.; Nagler, S. E.; Tennant, D. A.; Sales, B. C. and Barnes, T. *Phys. Rev. Lett.* **1997**, *79*, 745.